Hadley Cell Dynamics in an Axisymmetric Single-Layer Model: Effects of Parameterized Eddies and Equatorial Heating

PENGCHENG ZHANG,[a] NICHOLAS J. LUTSKO,[a] SPENCER A. HILL,[b] AND SHANG-PING XIE[a]

[a] *Scripps Institution of Oceanography, University of California San Diego, La Jolla, California*
[b] *Department of Earth and Atmospheric Sciences, City College of New York, New York, New York*

(Manuscript received 22 May 2025, in final form 20 October 2025, accepted 5 November 2025)

ABSTRACT: This study investigates how the zonal-mean Hadley cell responds to parameterized midlatitude eddy forcing and equatorial thermal perturbations using a minimal idealized axisymmetric single-layer model. Analytical results show that eddy forcing flattens the meridional profiles of zonal wind and temperature near the equator, leading to higher-order latitude dependence compared to the angular momentum–conserving (AMC) limit. Numerical simulations demonstrate that increasing eddy strength produces a stronger and wider Hadley cell, with a smooth transition from an AMC regime to an eddy-dominant regime. This transition is effectively characterized by the local Rossby number (Ro): Ro decreases rapidly with weak eddy forcing but becomes less responsive to further increases in eddy strength once the system enters the eddy-dominant regime. We further explore how the Hadley cell responds to equatorial thermal perturbations of varying width. In the AMC regime, narrow thermal forcing contracts the Hadley cell, while broader thermal forcing promotes poleward expansion. In contrast, in the eddy-dominant regime, the system responds more linearly to thermal forcing, so increasing the width of tropical forcing alone no longer leads to Hadley cell expansion. These results highlight the critical role of midlatitude eddies in modulating Hadley cell variability and its sensitivity to external forcing and provide a useful theoretical and idealized modeling framework for further exploration of eddy-mean flow interactions.

KEYWORDS: Hadley circulation; Idealized models; Tropics

1. Introduction

The Hadley circulation is a fundamental component of Earth's atmospheric general circulation, governing the large-scale transports of energy, moisture, and momentum and shaping both global climate patterns and regional weather systems. It is driven by meridional gradients in solar heating and features rising motion near the equator, where the intertropical convergence zone (ITCZ) is located (Wodzicki and Rapp 2016), and subsidence around 30°N/S, marking the subtropical dry zones (Held and Hou 1980; Hou 1998). Variability in this circulation has profound implications for key climate phenomena such as monsoons and subtropical aridity, with direct ecological and societal impacts (e.g., see Liang and Wang 1998; Burls et al. 2019). As a result, the Hadley circulation has been extensively studied, with past studies exploring its variability on different time scales, its responses to other modes of climate variability, and its evolution in past and projected future climates (Oort and Yienger 1996; Dima and Wallace 2003; Diaz and Bradley 2004; Hu and Fu 2007; Lu et al. 2007; Brierley et al. 2009; Ma et al. 2018; Seo et al. 2023; Kim et al. 2023; Lionello et al. 2024).

While often depicted as a thermally driven, zonal-mean meridional overturning circulation, the Hadley cell is strongly influenced by eddy activity—departures from the time mean and/or zonal mean that play a critical role in its dynamics. A substantial difference in Hadley cell structure was identified between axisymmetric and nonaxisymmetric primitive equation models, presumably due to the effect of baroclinic eddies (Kim and Lee 2001). Further, a large fraction of the isentropic mass flux of the Hadley circulation does not recirculate within the tropics but connects continuously to the extratropical eddy mass fluxes to form hemispheric-scale overturning circulations (e.g., see Fig. 1 in Walker and Schneider 2006). Eddy fluxes have been shown to substantially influence various aspects of the Hadley cells, including their strength, meridional extent, and responses to global warming (Kim and Lee 2001; Walker and Schneider 2006; Caballero 2007, 2008; Schneider and Bordoni 2008; Bordoni and Schneider 2010; Kang and Lu 2012; Adam and Harnik 2013; Singh et al. 2017; Davis and Birner 2022; Hill et al. 2022; Hasan et al. 2024).

A broad spectrum of models, from axisymmetric single-layer models to three-dimensional primitive equation models and fully coupled Earth system models, has been used to study Hadley cell dynamics (Maher et al. 2019). However, persistent challenges remain in examining the role of eddies, particularly in assessing sensitivity to varying eddy strength. Axisymmetric models, such as the seminal frameworks introduced by Held and Hou (1980) and Held (2000), have provided fundamental physical insights but are unable to explicitly represent eddy processes. In contrast, eddy effects in three-dimensional models are typically modulated indirectly by altering parameters such as planetary radius, rotation rate, thermal forcing, or convective relaxation profiles (e.g., Walker and Schneider 2006). These adjustments, however, introduce confounding changes

Pengcheng Zhang's current affiliation: Climate Systems Engineering initiative, The University of Chicago, Chicago, Illinois.

Corresponding author: Pengcheng Zhang, pczhang@uchicago.edu

DOI: 10.1175/JAS-D-25-0076.1

to Coriolis forces or meridional temperature gradients, complicating direct comparison with Earth's climate.

To address these limitations, intermediate approaches have been developed that enable diagnostic modeling of Hadley cell dynamics in idealized yet tunable frameworks, for example, by incorporating parameterized eddies into simplified axisymmetric models. This methodology was supported by Davis and Birner (2019), who demonstrated that prescribing time-mean eddy tendencies in an axisymmetric model can replicate nonaxisymmetric climate features, albeit within a relatively complex modeling framework. Sobel and Schneider (2009) introduced a parameterization for eddy momentum flux divergence in a highly idealized axisymmetric single-layer model and successfully reproduced key qualitative features of the Hadley cells in general circulation model (GCM) simulations. However, Sobel and Schneider (2009) did not explicitly test their parameterization against observations or systematically explore the sensitivity to eddy strength. As a result, the dynamics governing the transition from eddy-free to eddy-dominated regimes and the behaviors of the Hadley circulation across the corresponding spectrum of eddy forcing strengths in idealized models remain poorly understood.

In this study, we use a minimal axisymmetric single-layer model modified based on Sobel and Schneider (2009) to systematically investigate how eddies, originating from the midlatitudes, shape the dynamics of the zonal-mean Hadley cell. Analytical results reveal that parameterized eddies flatten the meridional gradients of zonal wind and temperature near the equator, leading to a higher-order latitude dependence than in the angular momentum–conserving limit. We then use numerical simulations to show that the Hadley cell strengthens and expands poleward in response to eddy forcing, consistent with findings from more complex models and existing theory (Caballero 2007; Schneider and Bordoni 2008). As eddy strength increases, the model exhibits a smooth and monotonic but nonlinear transition from an angular momentum–conserving (AMC) regime to an eddy-dominated regime. Finally, motivated by the observed modulation of Hadley cell extent by El Niño events (Oort and Yienger 1996; Seager et al. 2003; Lu et al. 2008) and ITCZ width (Watt-Meyer and Frierson 2019), we examine how the Hadley cell responds to equatorial thermal perturbations across these regimes. In the AMC regime, narrow perturbations contract the Hadley cell, while broader ones lead to expansion. However, in the eddy-dominant regime, the capacity to expand the Hadley cell through wider thermal perturbations alone diminishes.

The remainder of this paper is structured as follows. Section 2 introduces the numerical model and evaluates the effectiveness of the parameterization with observational data. Section 3 presents the analytical scaling behavior near the equator in response to parameterized eddies. Section 4 describes the Hadley cell responses to parameterized eddies of varied strength. Section 5 discusses how the Hadley cell's responses to equatorial thermal perturbations depend on eddy strength. Finally, section 6 provides a summary and conclusions.

2. Model description

We employ an axisymmetric single-layer model on an equatorial β plane adapted from Sobel and Schneider (2009, 2013) to simulate the upper troposphere.[1] The model equations are

$$\partial_t u - v(\beta y - \partial_y u) = -u(\partial_y v)\mathcal{H}(\partial_y v) - \mathcal{F} - \mathcal{S}, \tag{1}$$

$$2\partial_t v + \beta y u = -\frac{gH}{T_0}\partial_y T, \tag{2}$$

$$\partial_t \theta + \frac{h\Delta_z}{H}\partial_y v = \frac{\theta_E - \theta}{\tau}. \tag{3}$$

Here, u and v denote the zonal-mean zonal and meridional components of the wind velocity, respectively, within a thin layer of constant thickness h located just below the tropopause at height H. Under the β-plane approximation around the equator, the Coriolis force is $f = \beta y$. Potential temperature[2] θ and temperature T are related by $\theta = T(p_s/p_t)^{R/c_p}$, where the fixed surface and tropopause pressures p_s and p_t are chosen such that $(p_s/p_t)^{R/c_p} = 1.6$. Additional fixed parameters include the potential temperature difference Δ_z between the surface and tropopause, the surface temperature T_0, and the thermal relaxation time τ. The radiative equilibrium temperature θ_E is prescribed as a function of latitude:

$$\theta_E = \begin{cases} \theta_{00} - \Delta_y \sin^2\left(\dfrac{\pi y}{2y_1}\right) & \text{if } |y| < y_1, \\ \theta_{00} - \Delta_y & \text{if } |y| \geq y_1, \end{cases} \tag{4}$$

where $y_1 = 9439$ km ($\sim 85°$ of latitude), consistent with the setting in Sobel and Schneider (2009). A complete list of parameter values is given in Table 1.

The first term on the rhs of Eq. (1) represents momentum advection by mean vertical flow, where $\mathcal{H}$ is the Heaviside function; this formulation assumes that the mass injected into the upper layer carries zero zonal momentum, and the momentum exchange occurs only in the ascending region (Esler et al. 2000; Shell and Held 2004; Adam and Paldor 2009). The $\mathcal{F} = \epsilon_u u$ represents the frictional drag, and $\mathcal{S}$ represents the eddy momentum flux divergence (EMFD), parameterized as

$$\mathcal{S} = \nu_d \mathcal{H}(u)\mathrm{sgn}(y)\partial_y u, \tag{5}$$

where ν_d controls the magnitude of the parameterized EMFD (see Sobel and Schneider 2009 for a detailed explanation). The factor of 2 in the zonal wind tendency term of Eq. (2) results from the assumptions that the meridional velocities at the upper and lower layers are equal and opposite and that the bottom layer has the same thickness as the upper layer (see the appendix; Xian and Miller 2008; Sobel and Schneider 2009). The model also assumes the zonal velocity in the lower

[1] See also the appendix and Xian and Miller (2008) for a detailed derivation of model equations.

[2] The θ and T may be better interpreted as virtual potential temperature and virtual temperature, respectively, to account for the effect of vapor buoyancy; see Yang et al. (2022).

TABLE 1. Values of model parameters used in this study.

Parameter	Value	Definition
τ	37 days	Thermal relaxation time
H	16 km	Tropopause height
h	4 km	Depth of upper-tropospheric layer
T_0	300 K	Reference surface temperature
Δ_z	60 K	Vertical potential temperature stratification
Δ_y	50 K	Radiative equilibrium equator-pole temperature gradient
θ_{00}	330 K	Background tropospheric-mean potential temperature
ϵ_u	10^{-8} s^{-1}	Background Rayleigh drag
β	2×10^{-11} m^{-1} s^{-1}	Meridional gradient of Coriolis parameter

layer is negligible compared with that in the upper layer.[3] Since the model is highly idealized, we mostly focus on the nondimensional and/or qualitative features rather than the specific values of velocities in interpreting the model results.

Following Sobel and Schneider (2009) and Zhang and Lutsko (2022), we adopt a domain comprising 800 grid points with a horizontal resolution of 39.3 km. To ensure numerical stability, a second-order diffusion term that damps small-scale perturbations, including tropical gravity waves, is included in Eq. (2), although it is not explicitly shown. The model employs a leapfrog time-stepping scheme and is integrated over 15 model years for each simulation. Results presented in this study represent averages over the final 5 years of integration. Hereafter, unlike the expressions in the time-varying numerical model, all variable symbols denote temporal and zonal means without the explicit use of overbars or brackets.

We evaluate the effectiveness of the eddy parameterization using reanalysis data from the fifth generation European Centre for Medium-Range Weather Forecasts atmospheric reanalysis (ERA5; Hersbach et al. 2020). The diagnostic EMFD,

$$\mathrm{EMFD} = -\frac{1}{a\cos^2\phi}\frac{\partial}{\partial\phi}([\overline{u}^*\overline{v}^*]\cos^2\phi) - \frac{1}{a\cos^2\phi}\frac{\partial}{\partial\phi}([\overline{u'v'}]\cos^2\phi), \tag{6}$$

is treated as the ground truth and computed using hourly wind velocity at 150 hPa during 2004–23, where $[\cdot]$ denotes a zonal mean, $\bar{\cdot}$ denotes a temporal mean, $\cdot^*$ denotes a departure from the zonal mean, $\cdot'$ is a departure from the temporal mean, and a is Earth's radius. The diagnostic EMFD is averaged over the entire period, March–May (MAM) and September–November (SON), respectively, and then compared against the parameterized EMFD obtained via Eq. (5). Note that we focus on the equinox condition in this study, although this parameterization is designed to be compatible with cross-equatorial Hadley cells (Sobel and Schneider 2009).

As illustrated in Fig. 1, the parameterized EMFD at 150 hPa aligns well with the diagnostic results within the Hadley cell region from 5° to 30°S,[4] except for the contribution from equatorial planetary waves, which are excluded by design and lie outside the scope of this study. Similar comparisons are performed on 200 and 250 hPa, and the results are qualitatively the same within the Hadley cell (not shown). We focus on the Southern Hemisphere in this comparison, where the parameterization performs reasonably well. Its performance deteriorates in the Northern Hemisphere, presumably due to the parameterization [Eq. (5)] being incapable of dealing with easterly zonal wind in the deep tropics and/or more complex topography and land–sea contrasts in the higher latitudes of Northern Hemisphere. In the absence of a compelling explanation for this hemispheric asymmetry, the results presented here may be interpreted as more applicable to Earth's Southern Hemisphere.

3. Analysis of equilibrium scaling behaviors

The simplicity of the axisymmetric single-layer model allows an analytical examination of the scaling behavior of its equilibrated states. To do so, we neglect the time derivatives and set the friction term $\mathcal{F}$ to zero. For $y > 0$, the model equations reduce to

$$v(\beta y - \partial_y u) = u(\partial_y v)\mathcal{H}(\partial_y v) + v_d\partial_y u, \tag{7}$$

$$\beta y u = -\frac{gH}{T_0}\partial_y T, \tag{8}$$

$$\frac{h\Delta_z}{H}\partial_y v = \frac{\theta_E - \theta}{\tau}. \tag{9}$$

We focus only on the model's Northern Hemisphere to simplify the mathematical derivations, and the complete solution may be obtained based on hemispheric symmetry (u, T) or antisymmetry (v).

[3] This approximation does not hold strictly, as the surface velocity u_s, though much smaller than u, must be nonzero so the surface friction can balance the acceleration exerted by the upper layer; see Adam (2023) for a more physically consistent setup of bottom-layer momentum.

[4] Note that the parameterization [Eq. (5)] is designed for the EMFD inside the Hadley cell and does not work poleward of 30°S.

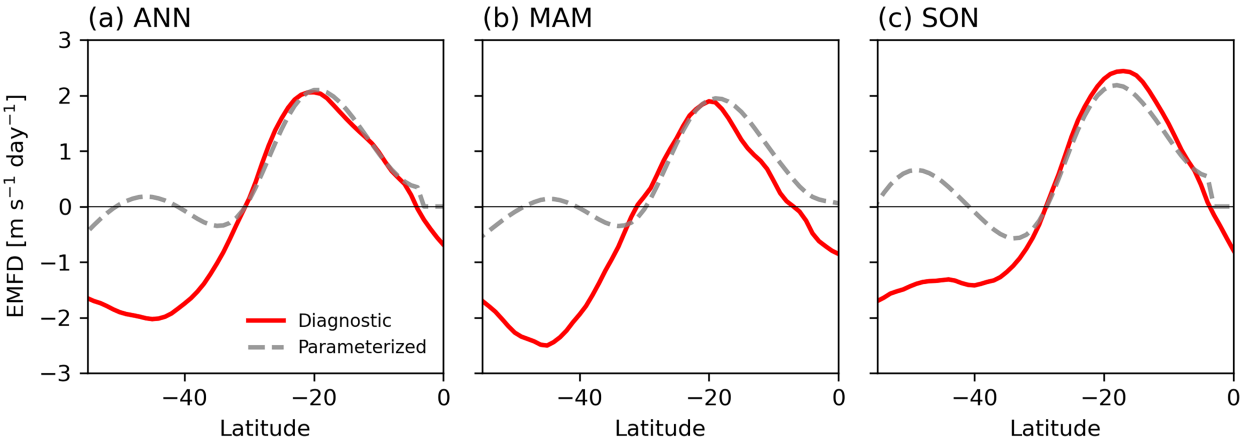

FIG. 1. Comparison of parameterized (gray dashed) and diagnostic (red solid) EMFD at 150 hPa in the Southern Hemisphere (m s^{-1} day^{-1}). The EMFD is averaged (a) annually, (b) in MAM, and (c) in SON, over a 20-yr period of 2004–23. The parameterized EMFD is calculated based on Eq. (5) with $v_d = 1.5$ m s^{-1}, and the diagnostic counterpart is calculated based on Eq. (6).

We consider four representative cases: 1) the canonical AMC regime, 2) a quasi-AMC regime with vertical momentum exchange but without eddy stress, 3) a non-AMC regime with eddy stress but without vertical momentum exchange, and 4) a non-AMC regime including both effects. Apart from eddy stress, the vertical momentum exchange is also examined here, as it modifies the wind and temperature profiles in a similar axisymmetric shallow-water model in Adam and Paldor (2010). We analyze solutions of the system for each case and then validate the analytical results with numerical simulations corresponding to each case (Fig. 2), using $v_d = 0.0125$ m s^{-1} for the amplitude of the parameterized EMFD. Note that, except for the simplest AMC case, an analytical solution to the model requires solving a fifth-order nonlinear ODE. While formal solutions may be technically possible, they are difficult to interpret and provide limited physical insight. Instead, we expand the zonal and meridional wind components, $u(y)$ and $v(y)$, as power series in y near the equator:

$$u = a_1 y + a_2 y^2 + a_3 y^3 + \cdots, \tag{10}$$

$$v = b_1 y + b_2 y^2 + b_3 y^3 + \cdots, \tag{11}$$

with $a_0 = b_0 = 0$ from equinoctial symmetry. Note that we are examining the Northern Hemisphere where $y > 0$; therefore, $a_1, a_3, \ldots$ and $b_2, b_4, \ldots$ may be nonzero despite that the zonal and meridional winds should be hemispherically symmetric and antisymmetric. The wind profiles for the Southern Hemisphere may be obtained as $u_{\mathrm{SH}}(y) = u(|y|)$ and $v_{\mathrm{SH}}(y) = -v(|y|)$ when $y < 0$. These series are presumed valid in a neighborhood around the equator, though similar expansions could, in principle, be constructed around the Hadley cell edge y_E. However, y_E is determined by integrating Eq. (8) and thus requires knowledge of the full solution.

In addition to u, v, and T, our analysis also considers the local Rossby number Ro:

$$\mathrm{Ro} = -\frac{\zeta}{f} = \frac{\partial_y u}{\beta y}, \tag{12}$$

which quantifies the proximity of the tropical circulation to the inviscid AMC limit and has been discussed in many previous studies of the Hadley circulation dynamics (Walker and Schneider 2006; Kang and Lu 2012; Adam and Harnik 2013; Hill et al. 2022).

a. The AMC regime

The angular momentum–conserving Hadley circulation has been extensively studied (Held and Hou 1980; Lindzen and Hou 1988; Hou and Lindzen 1992; Held 2000). A full solution of the AMC limit of the model ($v_d = 0$) is given in the appendix of Sobel and Schneider (2009), and we briefly summarize the main features of the solution here. Note that Sobel and Schneider (2009) adopted a parabolic form of $\theta_E(y)$, while we prefer a sinusoidal form in this study [Eq. (4)] to avoid discontinuities near the outer edge of Hadley cells.

In the AMC limit, the zonal momentum budget [Eq. (7)] simplifies to

$$v(\beta y - \partial_y u) = 0, \tag{13}$$

yielding the zonal wind profile $u_{\mathrm{AMC}}(y) = \beta y^2/2$ (see Fig. 2a) and a local Rossby number Ro = 1 throughout the Hadley cell. Given $u_{\mathrm{AMC}}(y)$, Eq. (8) can be integrated to obtain the corresponding meridional temperature profile, $T_{\mathrm{AMC}}(y)$, which can then be substituted into Eq. (9) to derive $v_{\mathrm{AMC}}(y)$. While we do not write out the full expressions here, we note, for reference, that $T_{\mathrm{AMC}}(y) = C_0 - C_4 y^4$ and $v_{\mathrm{AMC}}(y) \sim B_1 y + B_3 y^3 + B_5 y^5 + \cdots$, where the constants B_n and C_n are in principle solvable and determined by the outer boundary conditions at the Hadley cell edge.

A closed-form expression for $v_{\mathrm{AMC}}(y)$ is not available when using a sinusoidal form for $\theta_E(y)$; however, we can gain some intuition for the form of v_{AMC} by considering Eq. (9) and the radiative equilibrium temperature profile $\theta_E(y)$. First,

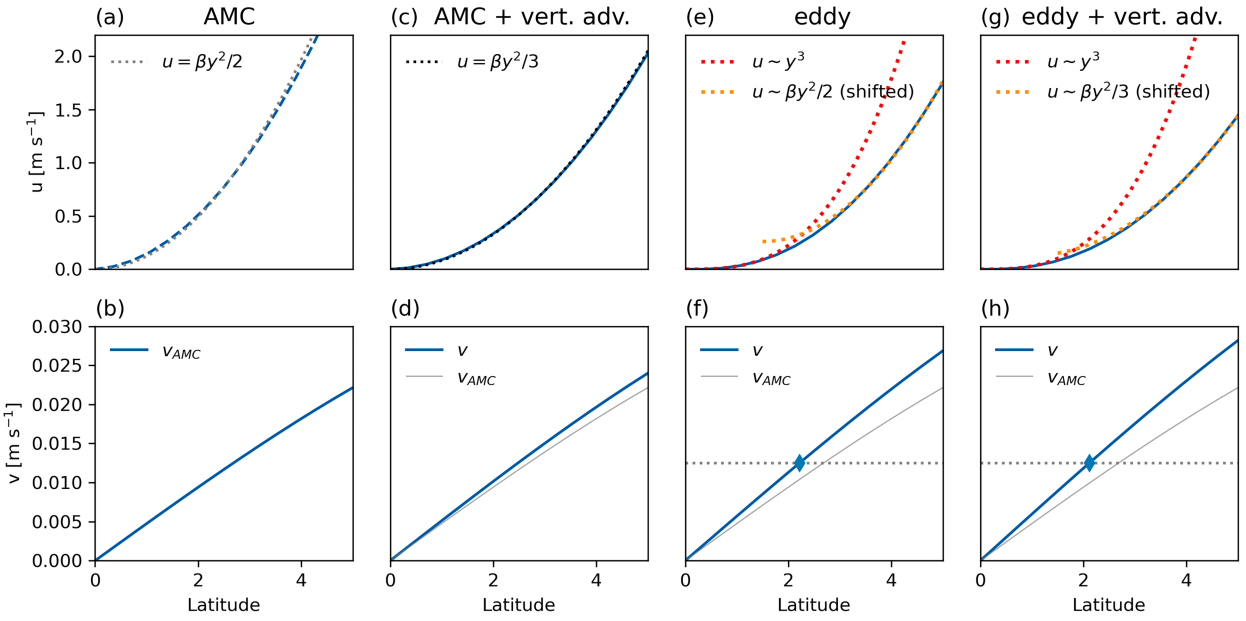

FIG. 2. Simulated zonal-mean zonal and meridional winds for (a),(b) a canonical AMC regime, (c),(d) a quasi-AMC regime including vertical momentum exchange, (e),(f) a non-AMC regime with eddy stress but without vertical momentum exchange, and (g),(h) a non-AMC regime including both eddy stress and vertical momentum exchange. The eddy parameter in (e)–(h) is set as $v_d = 0.0125$ m s^{-1}. The dotted curves in (a), (c), (e), and (g) are quadratic and cubic references indicated by the respective legend, and the gray dotted lines in (f) and (h) denote $v = v_d$. Note that the orange dotted curves in (e) and (g) are obtained by translating the graph of $u = \beta y^2/2$ and $u = \beta y^2/3$, respectively. The meridional wind profile in (b) is repeated in (d), (f), and (h) as gray curves for an easier comparison.

B_1 is set by the difference between the radiative equilibrium temperature at the equator $T_E(0)$ and the actual temperature at the equator $T_{\mathrm{AMC}}(0)$, i.e., $B_1 \propto T_E(0) - T_{\mathrm{AMC}}(0)$. Once non-AMC factors are included in the model, the flatter temperature profile with a lower $T(0)$ requires a larger v, as will be shown in the following analysis. Second, the fifth-order term $B_5 y^5$ in v_{AMC} comes from the integration of the difference between the fourth-order terms in $T_{\mathrm{AMC}}(y)$ and the Taylor expansion of $\theta_E(y)$, while the cubic term (also other higher-order terms) originates solely from the corresponding term in $\theta_E(y)$ and is largely insensitive to other model parameters.

b. *Effect of vertical momentum exchange*

When the deceleration due to vertical momentum transport is included, Eq. (13) becomes

$$\beta v y = v \partial_y u + u \partial_y v. \tag{14}$$

Substituting the power series expansions for $u(y)$ and $v(y)$ gives

$$b_1 \beta y^2 + \cdots = 2a_1 b_1 y + (3a_1 b_2 + 3a_2 b_1) y^2 + \cdots. \tag{15}$$

Equating the coefficients of like powers of y yields $a_1 = 0$ and $a_2 = \beta/3$. The zonal wind profile therefore becomes

$$u(y) = \frac{1}{3}\beta y^2 + \cdots, \tag{16}$$

indicating that while the vertical momentum transport reduces the magnitude of $u(y)$, it preserves its quadratic dependence on latitude. The temperature profile likewise retains the form $T(y) \sim C_0 - C_4 y^4$, though with altered coefficients. The slightly weaker winds imply a flatter temperature gradient, so while v retains the same form as in the AMC limit, its amplitude is slightly larger at a given latitude to compensate for the increased thermal transport demand. From our solution for $u(y)$, the local Rossby number Ro = 2/3, compared to unity in the canonical AMC case. As a validation, Fig. 2c demonstrates that the zonal wind profile from the numerical solution goes as $\beta y^2/3$ rather than $\beta y^2/2$ near the equator. The ratio of 2:3 between $u(y)$ in these two cases is consistent with the leading-order scalings in Adam and Paldor (2010), where the vertical momentum advection is enabled/disabled in an axisymmetric shallow-water model.

This result does not extend across the entire ascent region ($\partial_y v > 0$), since it relies on the validity of the leading-order approximation $v \sim b_1 y$, which breaks down near the half-width of the Hadley cell (roughly where $\partial_y v = 0$). Away from the ascent region, the flow is supposed to retain angular momentum conserving, with its meridional profile features a shifted AMC-like parabola (not shown).

c. *Effect of parameterized eddies*

When the parameterized EMFD is included, Eq. (13) becomes

$$\beta v y = (v + v_d)\partial_y u. \tag{17}$$

Substituting the power series expansions gives

$$b_1\beta y^2 + \cdots = a_1 v_d + (2a_2 v_d + a_1 b_1)y + (3a_3 v_d + a_1 b_2 + 2a_2 b_1)y^2 + \cdots. \quad (18)$$

Equating coefficients of like powers of y yields $a_1 = 0$, $a_2 = 0$, and $a_3 = b_1\beta/3v_d$. Consequently, the zonal wind profile becomes

$$u(y) = \frac{b_1\beta}{3v_d}y^3 + \cdots. \quad (19)$$

So, the zonal wind now increases with the cube of latitude, rather than quadratically. This scaling, in turn, implies a meridional temperature profile of the form $T(y) \sim C_0 - C_5 y^5$. These results indicate that parameterized eddies substantially alter the scaling behavior of both velocity and temperature fields, resulting in weaker meridional gradients near the equator. As discussed in the AMC case, despite remaining undetermined due to the absence of outer boundary conditions, the coefficient b_1 in $v(y)$ becomes larger because of a weaker meridional temperature gradient. The $v(y)$ will also have a term going as y^6 from the equilibrated temperature profile $T(y)$, as opposed to y^5 in the eddy-free regime.

The cubic dependence of $u(y)$ is expected to hold only in the vicinity of the equator. The local Rossby number $\mathrm{Ro} = \partial_y u/\beta y \sim b_1 y/v_d$ is zero at the equator and then increases with latitude, suggesting a gradual transition toward the AMC regime, where the zonal wind regains its quadratic form when v is much larger than v_d. For convenience, we define a critical latitude[5] y_c where $v = v_d$. Poleward of y_c where $v \gg v_d$, or where horizontal advection dominates over parameterized eddy forcing, $u(y)$ transitions from cubic back to quadratic dependence as the flow transitions to the AMC regime. Our numerical simulation with nonzero v_d confirms this behavior: Zonal wind follows a cubic profile near the equator and transitions to a quadratic one beyond y_c, which serves as an effective radius of convergence for Eq. (19) (Figs. 2e,f). As v_d approaches zero, y_c shifts equatorward, yielding a smooth transition to a purely quadratic regime. In the next section, we will see the region of cubic fitting expands poleward as v_d increases.

d. *Combined effect of vertical transport and parameterized eddies*

When both vertical momentum transport and parameterized eddies are included, the steady-state momentum equation for $y > 0$ becomes

$$\beta v y = v\partial_y u + u\partial_y v + v_d\partial_y u. \quad (20)$$

Substituting the power series expansions yields

$$b_1\beta y^2 + \cdots = a_1 v_d + (2a_2 v_d + 2a_1 b_1)y + (3a_3 v_d + 3a_1 b_2 + 3a_2 b_1)y^2 + \cdots. \quad (21)$$

Once again, we obtain $a_1 = 0$, $a_2 = 0$, and $a_3 = b_1\beta/3v_d$, and therefore,

$$u(y) = \frac{b_1\beta}{3v_d}y^3 + \cdots, \quad (22)$$

which is formally identical to the case with parameterized eddies alone. However, the coefficient b_1 will differ between the two cases: The additional vertical momentum transport will weaken the zonal wind and strengthen the meridional wind, consistent with the behavior observed in the eddy-free regime. The zonal wind profile from the simulation again shows a near-equatorial cubic dependence that transitions to a quadratic profile farther poleward, though with slightly reduced amplitude (Figs. 2g,h; cf. Figs. 2e,f).

Comparing the four cases above, the parameterized eddies substantially alter the scaling of the zonal wind from quadratic to cubic near the equator, while the inclusion of vertical momentum transport does not affect the scaling behavior, regardless of whether eddy forcing is present. This supports the conclusion—borne out in our simulations and in Sobel and Schneider (2009)—that Hadley cell dynamics are less sensitive to vertical momentum exchange than to parameterized eddies. Notably, even very weak eddies (small v_d) reduce the Rossby number Ro from 1 (or 2/3) to nearly zero at the equator. Away from the equator, Ro increases to a maximum in the center of the cell and then returns to zero at the cell edge where the zonal wind reaches maximum. Its maximum, along with the meridional slope of Ro near the equator, decreases as v_d increases, as will be shown in the following section.

4. Simulated effects of varying eddy strength

We now examine the effects of varying the parameterized eddy strength on the simulated Hadley circulation. These simulations allow us to investigate aspects of the flow we were unable to solve for analytically (e.g., the Hadley cell width and strength).

The axisymmetric single-layer model simulations are conducted with v_d varying from 0 to 2.5 m s^{-1}, and this set of simulations sufficiently covers Earth's eddy strength (see Hill et al. 2025), as indicated by the analysis of Rossby number later in this chapter. The resulting zonal wind u, meridional wind v, and temperature T are shown in Fig. 3 as functions of latitude. The zonal wind u within the Hadley cell is decelerated by the negative parameterized EMFD. Meanwhile, the meridional wind v, which represents the strength of the Hadley cell, increases as the additional eddy-induced deceleration in the tropics must be balanced by Coriolis acceleration [$\beta y v$ in Eq. (1)] in the zonal direction (Fig. 3b). If we define Hadley cell edge y_E as the latitude where u reaches

[5] Note that this y_c does not refer to the latitude of Rossby wave breaking or absorption where zonal wind speed matches the phase speed. Under the current eddy parameterization, the eddy momentum flux is assumed to extend to the equator.

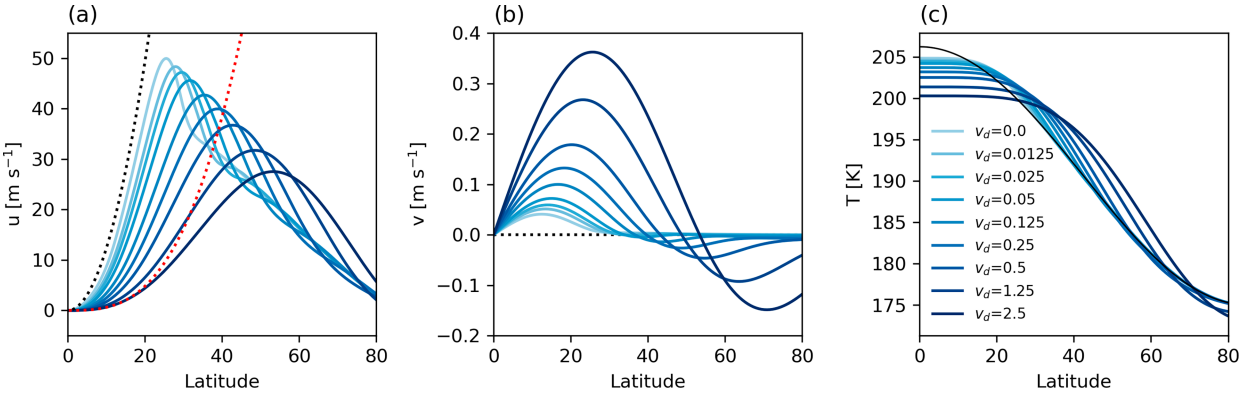

FIG. 3. Simulated zonal-mean (a) zonal wind, (b) meridional wind, and (c) temperature as functions of latitude. Darker color indicates stronger eddy strength. The dotted curves in (a) represent the AMC limit $u = \beta y^2/2$ (black) and $u \sim y^3$ fitting for $\upsilon_d = 2.5$ m s^{-1} (red), respectively. The black solid curve in (c) represents the radiative equilibrium temperature θ_E [Eq. (4)].

its maximum[6] and v drops to zero, then the EMFD is parameterized in a way of being positive (zonal deceleration) equatorward of y_E and negative (zonal acceleration) poleward of y_E [see Eq. (5)]; in other words, EMFD acts to extend the Hadley cell poleward (Figs. 3a,b). The maximum zonal wind $u(y_E)$ decreases because a larger Coriolis force at higher latitudes requires a smaller zonal velocity to keep geostrophic balance, provided the temperature gradient at y_E does not increase too much.[7] These responses in Hadley cell strength and extent are qualitatively consistent with results from more complex models (e.g., Kim and Lee 2001; Walker and Schneider 2006; Bordoni and Schneider 2010; Singh et al. 2017), further validating the ability of this simple single-layer model to capture Hadley cell responses to midlatitude eddies.

The equator-to-pole temperature gradient decreases as the eddy strength decreases (Fig. 3c), though we note that eddy heat transport is not explicitly included in the model equations and gravity waves are absent in the equilibrium state. This weakening of the equator-to-pole temperature gradient is primarily driven by the strengthening Hadley cell, which enhances ascent in the lower latitudes and transports low-entropy air from the bottom layer [Eq. (3)]. The resulting flattened temperature profile in the tropics suggests potential implications for the relationship between the weak temperature gradient (WTG) approximation (Sobel et al. 2001) and midlatitude eddies, though further exploration of this connection is beyond the scope of this study (see a relevant discussion in Held 1999).

As eddies become more influential, the profile of u deviates further from the AMC limit (black dotted curve in Fig. 3a). Note that the AMC limit cannot be fully reached even when $\upsilon_d = 0$ due to the effects of Rayleigh drag, vertical momentum transport, and unresolved eddies (e.g., numerical diffusion for stability). This deviation from the AMC limit is quantified by the local Rossby number $\mathrm{Ro} = \partial_y u/\beta y$. Figure 4a shows Ro as a function of latitude for all values of the eddy parameter υ_d. As eddy strength increases, Ro decreases throughout the Hadley cell, with its maximum value, marked by colored dots, dropping from approximately 0.9 to 0.1. Notably, the maximum Ro aligns with the latitude of maximum v, defined as y_m, regardless of eddy strength. When υ_d is small, Ro peaks where vertical momentum transport vanishes (i.e., where $\partial_y v$ changes sign). As υ_d increases, assuming vertical transport and Rayleigh drag are negligible, the zonal momentum balance,

$$v(\beta y - \partial_y u) \approx \upsilon_d \partial_y u, \tag{23}$$

yields the approximation

$$\mathrm{Ro} \approx \frac{v}{v + \upsilon_d}, \tag{24}$$

confirming that Ro peaks at y_m, the latitude where v peaks.

We now use the maximum Ro to quantify the overall strength of eddy stress within the Hadley cell. As the parameterization factor υ_d increases, the maximum Ro decreases, but this relationship is highly nonlinear: The reduction in Ro for υ_d increasing from 0 to 0.05 m s^{-1} is nearly the same as that for υ_d increasing from 0.05 to 2.5 m s^{-1} (Fig. 4b). The Ro is highly sensitive to υ_d when parameterized eddies are weak (AMC regime), where the dominant balance is

$$\beta y v \approx v \partial_y u. \tag{25}$$

As eddy effects become dominant (eddy-dominant regime), Ro becomes less sensitive to υ_d, with the dominant balance shifting to

$$\beta y v \approx \upsilon_d \partial_y u. \tag{26}$$

[6] Note that Menzel et al. (2024) suggest the relationship between the subtropical jet and Hadley cell is nuanced, as their variability is not necessarily coupled in realistic climate or more complex models.

[7] For a parabolic θ_E, $\partial_y T(y_E)$ increases faster and roughly balances the change of Coriolis parameter and $u(y_E)$ remains largely unchanged.

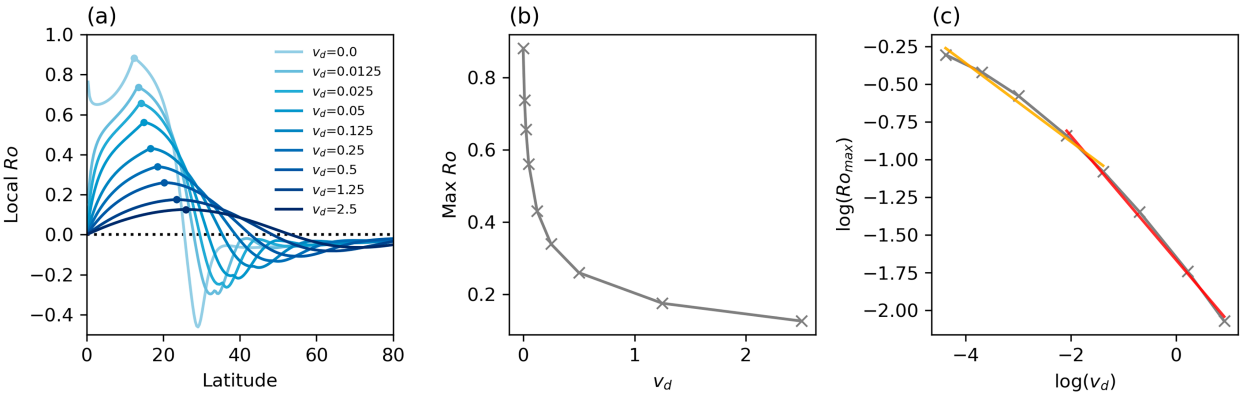

FIG. 4. (a) The local Ro as a function of latitude, with darker color indicating stronger eddy strength. (b) The maximum Ro, shown by solid dots in (a), as a function of increased eddy parameter ν_d. (c) As in (b), but in a log–log coordinate. The slope of the trend line in (c) is −0.26 (orange) and −0.41 (red).

Note that the nonlinear advection in the AMC regime [the rhs of Eq. (25)] is replaced by linear EMFD in the eddy-dominant regime [Eq. (26)]; therefore, the AMC and eddy-dominant regimes may also be classified as nonlinear and linear regimes, respectively. We will come back to this distinction in the next section. The transition between these regimes occurs around Ro = 0.5, where the governing momentum balance returns to the form of Eq. (23). Alternatively, defining the regime transition using the cell-mean Ro (Hill et al. 2025) yields qualitatively similar results (not shown).

The nonlinear relationship between the maximum Ro and ν_d suggests a possible power-law scaling of the form Ro $\sim \nu_d^\sigma$ with $\sigma < 0$ (Fig. 4b). Fitting the simulated maximum Ro against ν_d in log–log space yields scaling exponents of approximately $\sigma \approx -0.26$ at smaller ν_d and $\sigma \approx -0.41$ at larger ν_d (Fig. 4c), corresponding roughly to the AMC and eddy-dominant regimes discussed above. To interpret these scalings, we analyze the leading-order behavior of u, v, and T near the equator, although a full analytical solution across the entire Hadley cell remains unavailable.

Suppose that in the eddy-dominant regime, the leading-order approximations are $v(y) \sim b_1 y$ and $u(y) \sim b_1 \beta y^3/3\nu_d$ (see section 4), although higher-order terms become nonnegligible before reaching y_m. Assuming $y_E = 2y_m$, the leading-order approximation for the maximum local Rossby number is Ro $\sim b_1 y_m/\nu_d = b_1 y_E/2\nu_d$, and we seek to express b_1 and y_E in terms of ν_d. To proceed, we integrate the temperature profile to obtain

$$T(y) \sim C_0 - C_5' \frac{b_1}{\nu_d} y^5, \tag{27}$$

where C_5' represents a combination of known constants. For simplicity, we consider only the leading-order approximation of the radiative equilibrium temperature,

$$T_E(y) \sim C_E^{(0)} - C_E^{(2)} y^2, \tag{28}$$

where $C_E^{(0)}$ and $C_E^{(2)}$ are also the known constants. We assume $T(y)$ matches $T_E(y)$ at both y_m and y_E, an approximation borrowed from the equal-area model (Lindzen and Hou 1988), and the ascent branch is as wide as the descent one,[8] i.e., $y_E = 2y_m$, then we are able to obtain

$$\frac{b_1}{\nu_d} = \alpha y_E^{-3} \tag{29}$$

and

$$C_0 = -\gamma y_E^2 + C_E^{(0)}, \tag{30}$$

where $\alpha = 24C_E^{(2)}/31C_5'$ and $\gamma = C_E^{(2)} - \alpha C_5'$ are the known constants. From Eq. (9), we also notice that

$$b_1 \propto T_E(0) - T(0) \sim C_E^{(0)} - C_0 = \gamma y_E^2. \tag{31}$$

Combining Eqs. (29) and (31) yields $b_1 \sim \nu_d^{2/5}$, $y_E \sim \nu_d^{1/5}$, and thus, the maximum local Rossby number scales as

$$\text{Ro} \sim b_1 y_E/2\nu_d \sim \nu_d^{-2/5}. \tag{32}$$

Similarly, in the AMC regime, assuming $u(y) \sim b_1 \beta y^2/\nu_d$ and repeating the derivation, we obtain $b_1 \sim \nu_d^{1/2}$, $y_E \sim \nu_d^{1/4}$, and Ro $\sim \nu_d^{-1/4}$. These are in close agreement with the simulated maximum Ro scalings of $\nu_d^{-0.41}$ and $\nu_d^{-0.26}$ in the eddy-dominant and AMC regimes, respectively (Fig. 4).

This decrease of Ro sensitivity to parameterized eddy strength in the eddy-dominant regime is also seen in Adam and Harnik (2013), where the EMFD is represented more simply as a Newtonian drag, suggesting this varied sensitivity could be an intrinsic feature of the Hadley cell dynamics regardless of the specific representation of EMFD. Whether this change of sensitivity can be reproduced in models of

[8] This is valid in our model and confirmed with the numerical simulations but may not hold for moist cases where the ascent branch is narrower than the descent one.

different complexity remains an open question for future studies.

5. Hadley cell responses to tropical thermal perturbations

The response of the Hadley cell to tropical thermal perturbations has attracted considerable attention, largely due to the influence of the equatorial cold tongue and El Niño/La Niña events (e.g., see Oort and Yienger 1996; Amaya et al. 2018; Seo et al. 2023). Axisymmetric models have been widely used to investigate the Hadley cell's response to concentrated equatorial warming (Lindzen and Hou 1988; Hou and Lindzen 1992) and cooling (Adam 2023), although the role of midlatitude eddies remains largely unexplored. Moreover, while both El Niño and projected global warming involve enhanced tropical temperatures, their impacts on the Hadley circulation differ: El Niño, characterized by narrower warming, tends to contract the Hadley cell, whereas broader warming under climate change is accompanied by Hadley cell expansion (Lu et al. 2008). Tandon et al. (2013) found a consistent dependence of Hadley cell contraction or expansion on forcing width in GCMs; however, whether this dependence can be captured in an axisymmetric framework, and how it might be modulated by eddies of varying strength, remains an open question.

To address this question, we examine the impact of tropical thermal perturbations of varying width on Hadley cell contraction and expansion, considering how different strengths of parameterized midlatitude eddies modulate these responses. We introduce a thermal perturbation θ'_E superimposed on the radiative equilibrium temperature profile θ_E. The $\theta'_E(y)$ has a functional form same as $\theta_E(y)$ but is narrower in latitude and weaker in magnitude (Fig. 5a). The zonal wind profile without perturbation (black solid curve) and the wind response to the specific perturbation in Fig. 5a (gray dotted curve) are shown in Fig. 5b. In this case, the maximum wind response occurs equatorward of the background wind maximum (gray arrow in Fig. 5b), effectively contracting the Hadley cell.

To systematically explore this behavior, we conduct simulations across a wide range of eddy strengths and thermal perturbation widths. For each case, we calculate the latitudinal difference between the maxima of wind response and background wind—negative values indicating contraction and positive values indicating expansion—and plot the results in Fig. 6 as functions of eddy strength (represented by the maximum Ro of the background zonal wind profile) and half-width of the thermal perturbation. When eddy effects are weak (Ro $\sim$ 1), narrow perturbations contract the Hadley cell, whereas broader perturbations lead to expansion, consistent with the observed contrast between El Niño and global warming. However, as eddy influence strengthens (Ro $\to$ 0), the ability to expand the Hadley cell by broadening the thermal perturbation diminishes. This stark contrast between the AMC and eddy-dominant regimes underscores the role of midlatitude eddies in reshaping tropical forcing effects.

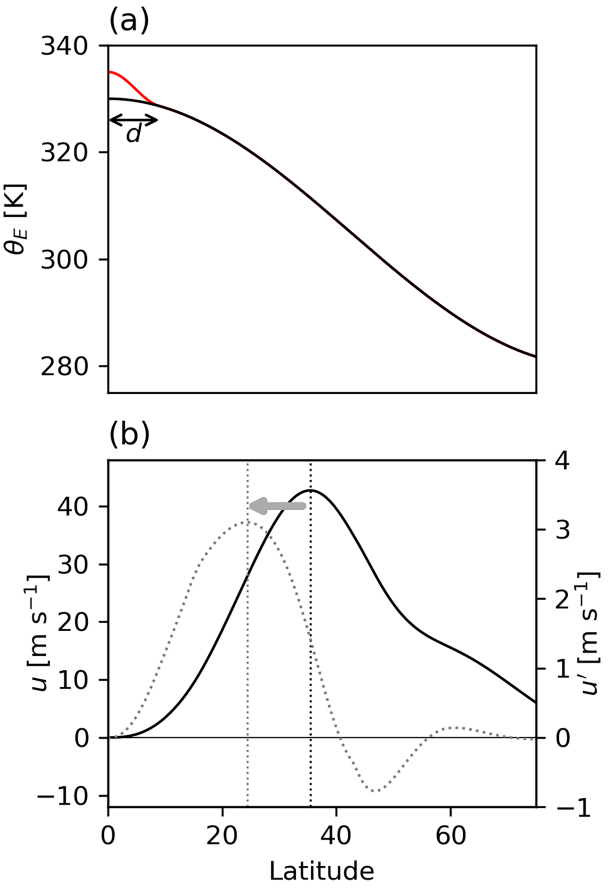

FIG. 5. (a) The profile of radiative equilibrium potential temperature θ_E [Eq. (4)] in black and the applied thermal perturbation θ'_E in red. The θ'_E shares the same functional form as θ_E but has different scales; in this case, the amplitude [equivalent to Δy in Eq. (4)] is 5 K and the half-width d (equivalent to y_1) is 10^3 km. (b) The background zonal wind without perturbation (solid) and the wind response to the thermal perturbation in (a) (dotted). The left and right vertical axes are for background wind (solid curve) and wind response (dotted curve), respectively. The vertical dotted lines indicate the latitudes of the curves' maxima. The $v_d = 0.05$ m s^{-1} in this example.

To explain the model's dependence on eddy strength in responding to equatorial thermal perturbations, we conceptualize the single-layer model as a function Φ that maps a given radiative equilibrium potential temperature profile $\boldsymbol{\theta}$ [subscript "E" is omitted, and boldface $\boldsymbol{\theta}$ is used to emphasize an array in latitude instead of $\theta(y)$ for simplicity] to a meridional zonal wind profile $\mathbf{u}$ (ignoring v and T for now), i.e.,

$$\mathbf{u} = \Phi(\boldsymbol{\theta}). \tag{33}$$

The anomalous zonal wind response $\mathbf{u}'$ to a thermal perturbation $\boldsymbol{\theta}'$ can then be expressed as

$$\mathbf{u}' = \Phi(\boldsymbol{\theta} + \boldsymbol{\theta}') - \Phi(\boldsymbol{\theta}) \tag{34}$$

$$= \Phi(\boldsymbol{\theta}') + \{\Phi(\boldsymbol{\theta} + \boldsymbol{\theta}') - [\Phi(\boldsymbol{\theta}) + \Phi(\boldsymbol{\theta}')]\}. \tag{35}$$

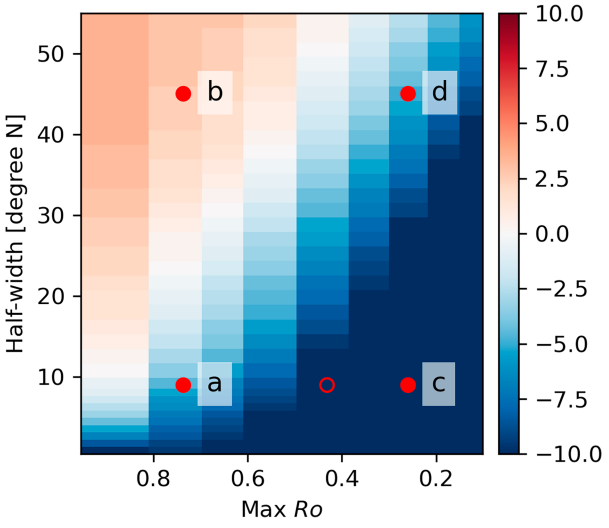

FIG. 6. The latitudinal difference between the maximum zonal wind response u' and background zonal wind profile u, with positive values indicating the zonal wind response u' expanding the Hadley cell poleward. The x axis denotes the maximum Ro of the background wind profile and is oriented such that values decrease to the right, emphasizing the strengthening of eddy stress in this direction. The y axis denotes the half-width of the thermal perturbation. The example in Fig. 5 is marked by the empty red circle. The filled red dots mark the four cases to be discussed below, with the adjacent letters labeling the corresponding panels in Fig. 7.

The degree of nonlinearity is formally quantified as

$$\mathrm{NL} := \Phi(\boldsymbol{\theta} + \boldsymbol{\theta}') - [\Phi(\boldsymbol{\theta}) + \Phi(\boldsymbol{\theta}')]. \tag{36}$$

In the eddy-dominant (or linear) regime, where nonlinear momentum advection—the primary source of model nonlinearity—is relatively weak, the nonlinear term can be neglected:

$$\mathbf{u}' \approx \Phi(\boldsymbol{\theta}'). \tag{37}$$

Since $\boldsymbol{\theta}$ and $\boldsymbol{\theta}'$ share the same functional form and differ only in scale, $\Phi(\boldsymbol{\theta}')$ peaks equatorward of $\Phi(\boldsymbol{\theta})$ as long as $\boldsymbol{\theta}'$ is narrower than the background profile $\boldsymbol{\theta}$, meaning that the zonal wind anomaly $\mathbf{u}'$ contracts the Hadley cell. Conversely, in the AMC (or nonlinear) regime, where the nonlinear term NL can no longer be neglected, it becomes possible for a perturbation $\boldsymbol{\theta}'$ narrower than the background $\boldsymbol{\theta}$ to generate a zonal wind anomaly $\mathbf{u}'$ that is wider than the background wind $\mathbf{u}$, thereby expanding the Hadley cell poleward.

To illustrate this mechanism, we evaluate four representative cases spanning weak versus strong eddy forcing (ν_d = 0.0125 vs 0.5 m s^{-1}) and narrow versus broad perturbation scales (half-width $d = 10^3$ vs 5×10^3 km), as shown in Fig. 7. These cases are marked by filled red dots in Fig. 6. Figure 7 presents the background zonal wind profile $\mathbf{u}$ (black solid curve) and the wind response $\mathbf{u}'$ (gray dotted curve) for each case, analogous to Fig. 5b but under different eddy strengths and perturbation widths. The linear component of the wind response, $\Phi(\boldsymbol{\theta}')$, is also simulated and plotted as a red dotted curve. We further calculate y_{diff} as the latitudinal difference of the peaks of full response $\mathbf{u}'$ and linear response $\Phi(\boldsymbol{\theta}')$, with larger y_{diff} representing stronger nonlinearity.

In the AMC regime, the full wind response $\mathbf{u}'$ deviates substantially from the linear response $\Phi(\boldsymbol{\theta}')$, with the latitudinal difference of their peaks y_{diff} being 7.8° and 8.7° for narrow and broad perturbations, respectively (Figs. 7a,b). Nonlinearity [Eq. (36)] effectively shifts $\Phi(\boldsymbol{\theta}')$ poleward (cf. gray and red dotted curves), and when the perturbation is broad enough (but still narrower than the background temperature profile), the full response $\mathbf{u}'$ can exceed the width of the background wind profile, expanding the Hadley cell—even when the linear response alone would suggest contraction (Fig. 7b). In contrast, in the eddy-dominant regime, as predicted, nonlinearity is weak, and the profiles of $\mathbf{u}'$ and $\Phi(\boldsymbol{\theta}')$ closely match in both shape and latitude of their maxima (Figs. 7c,d; y_{diff} = 2.8° and 3.1°, respectively, much smaller than in AMC regime). As a result, the full wind response $\mathbf{u}'$ still contracts the Hadley cell in both cases. Overall, the modeling results support our theoretical framework that explains why tropical forcing has different impacts depending on the dynamical regime of the Hadley circulation.

A natural question arises: Why does the model's nonlinearity tend to amplify, rather than dampen, the Hadley cell's expansion in response to tropical heating? Although a mathematically rigorous derivation is challenging, we offer a tentative but physically intuitive interpretation. The source of nonlinearity, i.e., the horizontal momentum advection ($-v\partial_y u$), acts to decelerate the zonal flow, with the strongest deceleration occurring near the center of the Hadley cell, where both v and $\partial_y u$ are largest. Outside the Hadley cell, where v diminishes, this nonlinear damping becomes negligible (see Fig. 3, particularly for small ν_d). Consequently, a hypothetical uniform increase in u would be preferentially damped within the Hadley cell interior but largely preserved outside it, effectively shifting the circulation poleward and leading to an apparent expansion.

One might argue that because stronger eddies both weaken the model's nonlinearity and widen the Hadley cell, it is the cell's width rather than its nonlinearity that enables narrow equatorial thermal forcing to expand the circulation. To test this possibility, we conducted simulations without parameterized eddies but varied the equator-to-pole temperature difference Δ_y from 50 to 85 K, thereby shifting the Hadley cell poleward while keeping it in the AMC (nonlinear) regime. In these experiments, the Hadley cell expanded in response to broad heating perturbations regardless of its initial width (not shown). We therefore conclude that the widening of the initial Hadley cell does not directly explain the changing sensitivity to equatorial thermal perturbations; instead, the key factor is the decay of model nonlinearity as ν_d increases.

6. Summary

This study investigates how the Hadley cell responds to midlatitude eddy momentum fluxes and equatorial thermal perturbations using an idealized axisymmetric single-layer

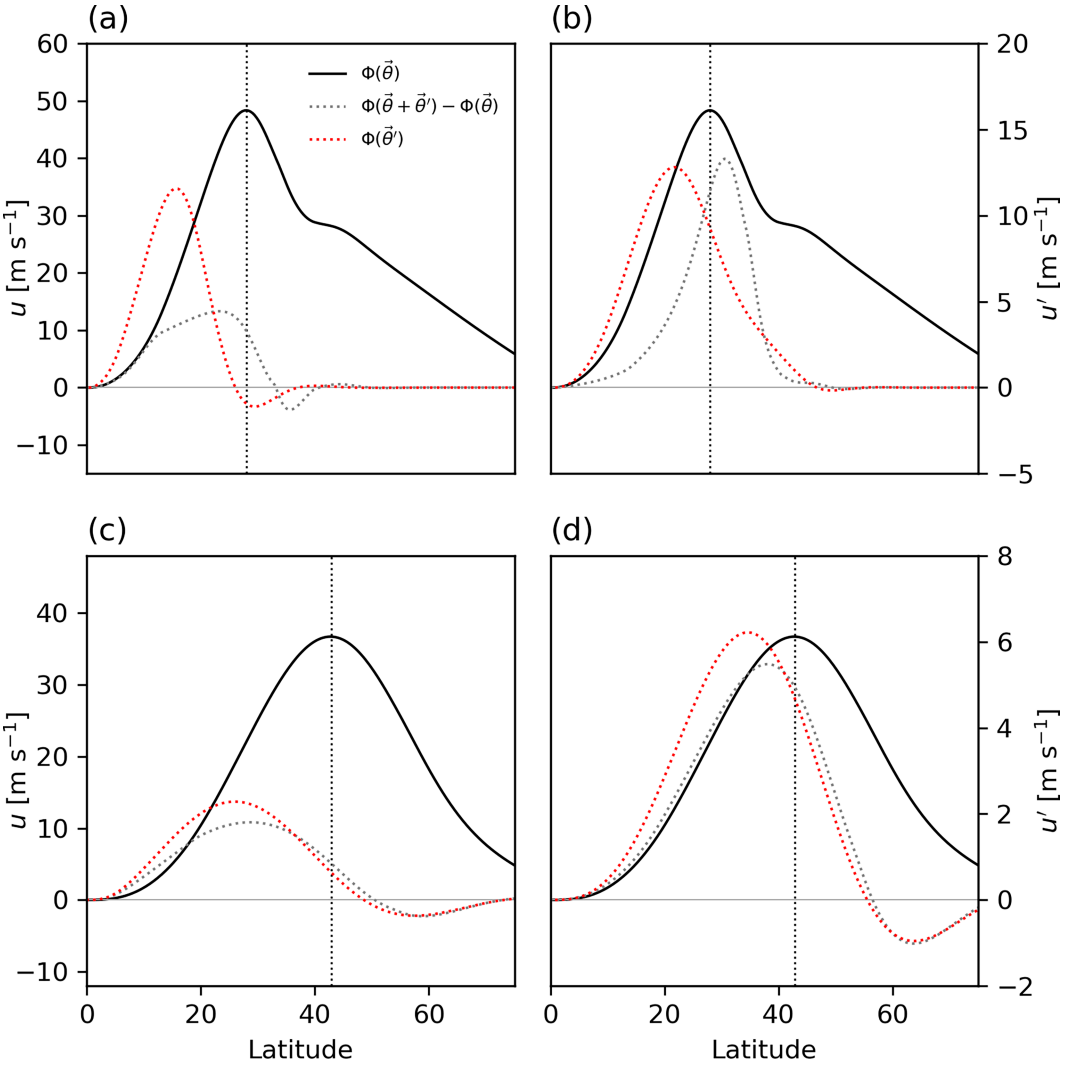

FIG. 7. The zonal wind profiles without equatorial thermal perturbation [$\Phi(\boldsymbol{\theta})$, black solid curves] and zonal wind responses to thermal perturbations [$\Phi(\boldsymbol{\theta}+\boldsymbol{\theta}')-\Phi(\boldsymbol{\theta})$, gray dotted curves] for different combinations of eddy strength and perturbation width: (a) $\upsilon_d = 0.0125$ m s^{-1} and $d = 10^3$ km, (b) $\upsilon_d = 0.0125$ m s^{-1} and $d = 5 \times 10^3$ km, (c) $\upsilon_d = 0.5$ m s^{-1} and $d = 10^3$ km, and (d) $\upsilon_d = 0.5$ m s^{-1} and $d = 5 \times 10^3$ km. See Fig. 6 for the distribution of these combinations in the Ro–d phase space. The red dotted curves show the model results for equatorial thermal perturbations only [without background radiative equilibrium temperature, i.e., $\Phi(\boldsymbol{\theta}')$]. The left and right vertical axes are for background wind (solid curves) and wind response (dotted curves), respectively. The vertical dotted lines show the latitudes of maximum background zonal winds.

model with parameterized eddy forcing. By combining analytical techniques with numerical simulations, we reveal how eddy momentum flux divergence systematically modifies the meridional structure of the tropical circulation and alters the Hadley cell's sensitivity to equatorial thermal forcing.

We begin by analyzing the model's equilibrium scaling behavior. Without parameterized eddies, the zonal wind follows a quadratic profile with latitude, consistent with the angular momentum–conserving (AMC) regime. Vertical momentum transport reduces the wind amplitude but preserves the quadratic form. In contrast, parameterized eddies introduce a cubic dependence near the equator, with weaker temperature gradients and a critical latitude beyond which the flow reverts to quadratic scaling. Importantly, the cubic dependence induced by parameterized eddies holds regardless of the presence of vertical momentum transport.

We then explore how the Hadley cell evolves across a wide range of eddy strengths. As the eddy forcing increases, the zonal wind weakens, the meridional flow intensifies, and the cell expands poleward. These changes are effectively captured by the local Rossby number (Ro), which serves as a compact, physically meaningful metric for tracking the relative importance of eddy effects. Ro decreases as eddy strength increases and characterizes the system's transition from AMC (Ro ~ 1)

to eddy-dominant (Ro ~ 0) regimes. This transition is smooth but nonlinear, as the maximum Ro drops sharply with initial inclusion of weak eddies in the AMC regime but later becomes less sensitive to ν_d in the eddy-dominant regime. This nonlinear behavior is characterized by a negative power scaling relationship between maximum Ro and ν_d, confirmed by numerical simulations and analytical derivations.

Finally, we examine how tropical thermal perturbations of varying meridional widths affect the Hadley cell under different eddy regimes. In the AMC regime, narrow perturbations contract the Hadley cell, while broader ones promote poleward expansion—behavior that aligns with the apparent contrast between El Niño–induced contraction and projected Hadley cell expansion under global warming. In the eddy-dominant regime, however, the response becomes nearly linear, and broadening the thermal forcing alone is insufficient to induce expansion. This contrast is explained through a decomposition of the model response: Nonlinearity in the AMC regime allows narrow forcing to generate a broad wind anomaly, a mechanism that might be suppressed when eddies dominate.

This study offers a minimal yet dynamically rich framework for understanding Hadley cell responses to both midlatitude eddies and equatorial forcing. While our focus is on equinox conditions, the seasonal cycle and its influence on eddy stress and momentum budgets is a natural extension for future work (Vimont et al. 2001; Simpson et al. 2014; Hill et al. 2021, 2022, 2025). Although our power series method is confined to the equatorial region, the results provide a solid theoretical basis for further exploration of Hadley cell dynamics across diverse parameter regimes. Additionally, our model omits eddy heat transport, influence of surface zonal wind, and explicit wave dynamics yet instead relies on a simple parameterization of the eddy momentum flux proportional to the subtropical wind speed. While this idealization facilitates analytical progress, future work may benefit from more physically grounded representation of eddy momentum and heat flux, for example, informed by careful inspection of eddy phase speed cospectra (e.g., see Moon and Cho 2020; Lorenz 2022; Adam 2023; Moon and Wettlaufer 2025).

Our model results suggest that in an eddy-dominant regime, it is difficult for a broad tropical warming perturbation to drive Hadley cell expansion. This stands in contrast to projections of global warming, which also feature enhanced tropical temperatures but are nonetheless robustly associated with Hadley cell expansion (e.g., see Korty and Schneider 2008; Vallis et al. 2015; Chemke and Polvani 2019). One possible reason for this discrepancy is that our simplified model does not account for the eddy feedback due to changes in baroclinic instability or subtropical static stability, which has been proven to be important in the Hadley cell response to tropical heating in a three-dimensional GCM (Sun et al. 2013). How to incorporate such midlatitude changes and reconcile them with the present framework remains an open question.

Acknowledgments. The authors thank Professors Adam Sobel, Tapio Schneider, Tiffany Shaw, and Da Yang for insightful discussions and thank Professor Isaac Held for constructive comments on an early version of the manuscript.

Data availability statement. The hourly ERA5 data are available at Copernicus Climate Data Store (https://doi.org/10.24381/cds.bd0915c6). The source codes of the numerical model are publicly available at https://github.com/zpcllyj/SobelSchneiderModel.

APPENDIX

Derivation of the Meridional Momentum Equation

Here is a brief derivation of Eq. (2), adapted from Xian and Miller (2008). Ignoring the advection term, the meridional momentum equation is

$$\frac{\partial v^*}{\partial t} = -fu^* - \frac{\partial \Phi}{\partial y}, \tag{A1}$$

where the notations u^* and v^* represent general winds at any altitude, as opposed to u and v for the upper layer. To introduce temperature, we apply ∂/∂_{z^*} to the above equation where z^* is pseudoheight:

$$z^* = \frac{RT_0}{g} \ln\left(\frac{p}{p_s}\right), \tag{A2}$$

where T_0 is reference surface temperature. Note that

$$dz^* = \frac{RT_0}{g} d(\ln p), \tag{A3}$$

and from hydrostatic balance, the differential of true height is

$$dz = \frac{RT}{g} d(\ln p), \tag{A4}$$

then the original equation becomes

$$\frac{\partial^2 v^*}{\partial t \partial z^*} = -f\frac{\partial u^*}{\partial z^*} - \frac{\partial}{\partial y}\left(\frac{\partial \Phi}{\partial z}\frac{\partial z}{\partial z^*}\right) = -f\frac{\partial u^*}{\partial z^*} - g\frac{\partial}{\partial y}\left(\frac{T}{T_0}\right). \tag{A5}$$

We then integrate the above equation from 0 to H:

$$\frac{\partial}{\partial t}[v^*(H) - v^*(0)] = -f[u^*(H) - u^*(0)] - \frac{g}{T_0}\frac{\partial \overline{T}}{\partial y}, \tag{A6}$$

where $\overline{T}$ is the vertically average temperature. The model assumes that the meridional velocities at the upper and bottom layers are equal and opposite, and the bottom layer has the same thickness as the upper layer. Also, we consider $u^*(H) \gg u^*(0)$ and assume a fixed lapse rate of the troposphere; then, the equation becomes

$$\frac{\partial}{\partial t}[v - (-v)] = -f(u - 0) - \frac{g}{T_0}\frac{\partial T}{\partial y}, \tag{A7}$$

$$2\frac{\partial v}{\partial t} = -fu - \frac{g}{T_0}\frac{\partial T}{\partial y}. \tag{A8}$$

The final form is used in the axisymmetric model in this study.

REFERENCES

Adam, O., 2023: The influence of equatorial cooling on axially symmetric atmospheric circulation forced by annually averaged heating. *J. Climate*, **36**, 7451–7464, https://doi.org/10.1175/JCLI-D-23-0157.1.

——, and N. Paldor, 2009: Global circulation in an axially symmetric shallow water model forced by equinoctial differential heating. *J. Atmos. Sci.*, **66**, 1418–1433, https://doi.org/10.1175/2008JAS2685.1.

——, and ——, 2010: Global circulation in an axially symmetric shallow-water model, forced by off-equatorial differential heating. *J. Atmos. Sci.*, **67**, 1275–1286, https://doi.org/10.1175/2009JAS3324.1.

——, and N. Harnik, 2013: Idealized annually averaged macroturbulent Hadley circulation in a shallow-water model. *J. Atmos. Sci.*, **70**, 284–302, https://doi.org/10.1175/JAS-D-12-072.1.

Amaya, D. J., N. Siler, S.-P. Xie, and A. J. Miller, 2018: The interplay of internal and forced modes of Hadley cell expansion: Lessons from the global warming hiatus. *Climate Dyn.*, **51**, 305–319, https://doi.org/10.1007/s00382-017-3921-5.

Bordoni, S., and T. Schneider, 2010: Regime transitions of steady and time-dependent Hadley circulations: Comparison of axisymmetric and eddy-permitting simulations. *J. Atmos. Sci.*, **67**, 1643–1654, https://doi.org/10.1175/2009JAS3294.1.

Brierley, C. M., A. V. Fedorov, Z. Liu, T. D. Herbert, K. T. Lawrence, and J. P. LaRiviere, 2009: Greatly expanded tropical warm pool and weakened Hadley circulation in the early Pliocene. *Science*, **323**, 1714–1718, https://doi.org/10.1126/science.1167625.

Burls, N. J., R. C. Blamey, B. A. Cash, E. T. Swenson, A. A. Fahad, M.-J. M. Bopape, D. M. Straus, and C. J. C. Reason, 2019: The Cape Town "Day Zero" drought and Hadley cell expansion. *npj Climate Atmos. Sci.*, **2**, 27, https://doi.org/10.1038/s41612-019-0084-6.

Caballero, R., 2007: Role of eddies in the interannual variability of Hadley cell strength. *Geophys. Res. Lett.*, **34**, L22705, https://doi.org/10.1029/2007GL030971.

——, 2008: Hadley cell bias in climate models linked to extratropical eddy stress. *Geophys. Res. Lett.*, **35**, L18709, https://doi.org/10.1029/2008GL035084.

Chemke, R., and L. M. Polvani, 2019: Exploiting the abrupt 4 × CO_2 scenario to elucidate tropical expansion mechanisms. *J. Climate*, **32**, 859–875, https://doi.org/10.1175/JCLI-D-18-0330.1.

Davis, N. A., and T. Birner, 2019: Eddy influences on the Hadley circulation. *J. Adv. Model. Earth Syst.*, **11**, 1563–1581, https://doi.org/10.1029/2018MS001554.

——, and ——, 2022: Eddy-mediated Hadley cell expansion due to axisymmetric angular momentum adjustment to greenhouse gas forcings. *J. Atmos. Sci.*, **79**, 141–159, https://doi.org/10.1175/JAS-D-20-0149.1.

Diaz, H. F., and R. S. Bradley, Eds., 2004: *The Hadley Circulation: Present, Past and Future.* Advances in Global Change Research, Vol. 21, Springer, 522 pp., https://doi.org/10.1007/978-1-4020-2944-8.

Dima, I. M., and J. M. Wallace, 2003: On the seasonality of the Hadley cell. *J. Atmos. Sci.*, **60**, 1522–1527, https://doi.org/10.1175/1520-0469(2003)060<1522:OTSOTH>2.0.CO;2.

Esler, J. G., L. M. Polvani, and R. A. Plumb, 2000: The effect of a Hadley circulation on the propagation and reflection of planetary waves in a simple one-layer model. *J. Atmos. Sci.*, **57**, 1536–1556, https://doi.org/10.1175/1520-0469(2000)057<1536:TEOAHC>2.0.CO;2.

Hasan, M., S. M. Larson, K. McMonigal, W. A. Robinson, and A. Aiyyer, 2024: Hemisphere-dependent impacts of ENSO and atmospheric eddies on Hadley circulation. *J. Climate*, **37**, 6533–6548, https://doi.org/10.1175/JCLI-D-24-0112.1.

Held, I. M., 1999: The macroturbulence of the troposphere. *Tellus*, **51A**, 59–70, https://doi.org/10.3402/tellusa.v51i1.12306.

——, 2000: The general circulation of the atmosphere. WHOI GFD Program, 70 pp., https://www.gfdl.noaa.gov/wp-content/uploads/files/user_files/ih/lectures/woods_hole.pdf.

——, and A. Y. Hou, 1980: Nonlinear axially symmetric circulations in a nearly inviscid atmosphere. *J. Atmos. Sci.*, **37**, 515–533, https://doi.org/10.1175/1520-0469(1980)037<0515:NASCIA>2.0.CO;2.

Hersbach, H., and Coauthors, 2020: The ERA5 global reanalysis. *Quart. J. Roy. Meteor. Soc.*, **146**, 1999–2049, https://doi.org/10.1002/qj.3803.

Hill, S. A., S. Bordoni, and J. L. Mitchell, 2021: Solsticial Hadley cell ascending edge theory from supercriticality. *J. Atmos. Sci.*, **78**, 1999–2011, https://doi.org/10.1175/JAS-D-20-0341.1.

——, ——, and ——, 2022: A theory for the Hadley cell descending and ascending edges throughout the annual cycle. *J. Atmos. Sci.*, **79**, 2515–2528, https://doi.org/10.1175/JAS-D-21-0328.1.

——, ——, ——, and J. M. Lora, 2025: Interpreting seasonal and interannual Hadley cell descending edge migrations via the cell-mean Rossby number. *J. Climate*, **38**, 5505–5520, https://doi.org/10.1175/JCLI-D-24-0678.1.

Hou, A. Y., 1998: Hadley circulation as a modulator of the extratropical climate. *J. Atmos. Sci.*, **55**, 2437–2457, https://doi.org/10.1175/1520-0469(1998)055<2437:HCAAMO>2.0.CO;2.

——, and R. S. Lindzen, 1992: The influence of concentrated heating on the Hadley circulation. *J. Atmos. Sci.*, **49**, 1233–1241, https://doi.org/10.1175/1520-0469(1992)049<1233:TIOCHO>2.0.CO;2.

Hu, Y., and Q. Fu, 2007: Observed poleward expansion of the Hadley circulation since 1979. *Atmos. Chem. Phys.*, **7**, 5229–5236, https://doi.org/10.5194/acp-7-5229-2007.

Kang, S. M., and J. Lu, 2012: Expansion of the Hadley cell under global warming: Winter versus summer. *J. Climate*, **25**, 8387–8393, https://doi.org/10.1175/JCLI-D-12-00323.1.

Kim, H.-K., and S. Lee, 2001: Hadley cell dynamics in a primitive equation model. Part II: Nonaxisymmetric flow. *J. Atmos. Sci.*, **58**, 2859–2871, https://doi.org/10.1175/1520-0469(2001)058<2859:HCDIAP>2.0.CO;2.

Kim, S.-Y., and Coauthors, 2023: Hemispherically asymmetric Hadley cell response to CO_2 removal. *Sci. Adv.*, **9**, eadg1801, https://doi.org/10.1126/sciadv.adg1801.

Korty, R. L., and T. Schneider, 2008: Extent of Hadley circulations in dry atmospheres. *Geophys. Res. Lett.*, **35**, L23803, https://doi.org/10.1029/2008GL035847.

Liang, X.-Z., and W.-C. Wang, 1998: Associations between China monsoon rainfall and tropospheric jets. *Quart. J. Roy. Meteor. Soc.*, **124**, 2597–2623, https://doi.org/10.1002/qj.49712455204.

Lindzen, R. S., and A. V. Hou, 1988: Hadley circulations for zonally averaged heating centered off the equator. *J. Atmos. Sci.*, **45**, 2416–2427, https://doi.org/10.1175/1520-0469(1988)045<2416:HCFZAH>2.0.CO;2.

Lionello, P., R. D'Agostino, D. Ferreira, H. Nguyen, and M. S. Singh, 2024: The Hadley circulation in a changing climate. *Ann. N. Y. Acad. Sci.*, **1534**, 69–93, https://doi.org/10.1111/nyas.15114.

Lorenz, D. J., 2022: The role of barotropic versus baroclinic feedbacks on the eddy response to annular mode zonal wind

anomalies. *J. Atmos. Sci.*, **79**, 2529–2547, https://doi.org/10.1175/JAS-D-22-0061.1.

Lu, J., G. A. Vecchi, and T. Reichler, 2007: Expansion of the Hadley cell under global warming. *Geophys. Res. Lett.*, **34**, L06805, https://doi.org/10.1029/2006GL028443.

——, G. Chen, and D. M. W. Frierson, 2008: Response of the zonal mean atmospheric circulation to El Niño versus global warming. *J. Climate*, **21**, 5835–5851, https://doi.org/10.1175/2008JCLI2200.1.

Ma, J., R. Chadwick, K.-H. Seo, C. Dong, G. Huang, G. R. Foltz, and J. H. Jiang, 2018: Responses of the tropical atmospheric circulation to climate change and connection to the hydrological cycle. *Annu. Rev. Earth Planet. Sci.*, **46**, 549–580, https://doi.org/10.1146/annurev-earth-082517-010102.

Maher, P., and Coauthors, 2019: Model hierarchies for understanding atmospheric circulation. *Rev. Geophys.*, **57**, 250–280, https://doi.org/10.1029/2018RG000607.

Menzel, M. E., D. W. Waugh, Z. Wu, and T. Reichler, 2024: Replicating the Hadley cell edge and subtropical jet latitude disconnect in idealized atmospheric models. *Wea. Climate Dyn.*, **5**, 251–261, https://doi.org/10.5194/wcd-5-251-2024.

Moon, W., and J. Y.-K. Cho, 2020: A balanced state consistent with planetary-scale motion for quasi-geostrophic dynamics. *Tellus*, **72A**, 1697164, https://doi.org/10.1080/16000870.2019.1697164.

——, and J. S. Wettlaufer, 2025: Midlatitude interactions expand the Hadley circulation. *J. Atmos. Sci.*, **82**, 1057–1071, https://doi.org/10.1175/JAS-D-24-0099.1.

Oort, A. H., and J. J. Yienger, 1996: Observed interannual variability in the Hadley circulation and its connection to ENSO. *J. Climate*, **9**, 2751–2767, https://doi.org/10.1175/1520-0442(1996)009<2751:OIVITH>2.0.CO;2.

Schneider, T., and S. Bordoni, 2008: Eddy-mediated regime transitions in the seasonal cycle of a Hadley circulation and implications for monsoon dynamics. *J. Atmos. Sci.*, **65**, 915–934, https://doi.org/10.1175/2007JAS2415.1.

Seager, R., N. Harnik, Y. Kushnir, W. Robinson, and J. Miller, 2003: Mechanisms of hemispherically symmetric climate variability. *J. Climate*, **16**, 2960–2978, https://doi.org/10.1175/1520-0442(2003)016<2960:MOHSCV>2.0.CO;2.

Seo, K.-H., S.-P. Yoon, J. Lu, Y. Hu, P. W. Staten, and D. M. W. Frierson, 2023: What controls the interannual variation of Hadley cell extent in the Northern Hemisphere: Physical mechanism and empirical model for edge variation. *npj Climate Atmos. Sci.*, **6**, 204, https://doi.org/10.1038/s41612-023-00533-w.

Shell, K. M., and I. M. Held, 2004: Abrupt transition to strong superrotation in an axisymmetric model of the upper troposphere. *J. Atmos. Sci.*, **61**, 2928–2935, https://doi.org/10.1175/JAS-3312.1.

Simpson, I. R., T. A. Shaw, and R. Seager, 2014: A diagnosis of the seasonally and longitudinally varying midlatitude circulation response to global warming. *J. Atmos. Sci.*, **71**, 2489–2515, https://doi.org/10.1175/JAS-D-13-0325.1.

Singh, M. S., Z. Kuang, and Y. Tian, 2017: Eddy influences on the strength of the Hadley circulation: Dynamic and thermodynamic perspectives. *J. Atmos. Sci.*, **74**, 467–486, https://doi.org/10.1175/JAS-D-16-0238.1.

Sobel, A. H., and T. Schneider, 2009: Single-layer axisymmetric model for a Hadley circulation with parameterized eddy momentum forcing. *J. Adv. Model. Earth Syst.*, **1**, 10, https://doi.org/10.3894/JAMES.2009.1.10.

——, and ——, 2013: Correction to "single-layer axisymmetric model for a Hadley circulation with parameterized eddy momentum forcing". *J. Adv. Model. Earth Syst.*, **5**, 654–657, https://doi.org/10.1002/jame.20030.

——, J. Nilsson, and L. M. Polvani, 2001: The weak temperature gradient approximation and balanced tropical moisture waves. *J. Atmos. Sci.*, **58**, 3650–3665, https://doi.org/10.1175/1520-0469(2001)058<3650:TWTGAA>2.0.CO;2.

Sun, L., G. Chen, and J. Lu, 2013: Sensitivities and mechanisms of the zonal mean atmospheric circulation response to tropical warming. *J. Atmos. Sci.*, **70**, 2487–2504, https://doi.org/10.1175/JAS-D-12-0298.1.

Tandon, N. F., E. P. Gerber, A. H. Sobel, and L. M. Polvani, 2013: Understanding Hadley cell expansion versus contraction: Insights from simplified models and implications for recent observations. *J. Climate*, **26**, 4304–4321, https://doi.org/10.1175/JCLI-D-12-00598.1.

Vallis, G. K., P. Zurita-Gotor, C. Cairns, and J. Kidston, 2015: Response of the large-scale structure of the atmosphere to global warming. *Quart. J. Roy. Meteor. Soc.*, **141**, 1479–1501, https://doi.org/10.1002/qj.2456.

Vimont, D. J., D. S. Battisti, and A. C. Hirst, 2001: Footprinting: A seasonal connection between the tropics and mid-latitudes. *Geophys. Res. Lett.*, **28**, 3923–3926, https://doi.org/10.1029/2001GL013435.

Walker, C. C., and T. Schneider, 2006: Eddy influences on Hadley circulations: Simulations with an idealized GCM. *J. Atmos. Sci.*, **63**, 3333–3350, https://doi.org/10.1175/JAS3821.1.

Watt-Meyer, O., and D. M. W. Frierson, 2019: ITCZ width controls on Hadley cell extent and eddy-driven jet position and their response to warming. *J. Climate*, **32**, 1151–1166, https://doi.org/10.1175/JCLI-D-18-0434.1.

Wodzicki, K. R., and A. D. Rapp, 2016: Long-term characterization of the Pacific ITCZ using TRMM, GPCP, and ERA-interim. *J. Geophys. Res. Atmos.*, **121**, 3153–3170, https://doi.org/10.1002/2015JD024458.

Xian, P., and R. L. Miller, 2008: Abrupt seasonal migration of the ITCZ into the summer hemisphere. *J. Atmos. Sci.*, **65**, 1878–1895, https://doi.org/10.1175/2007JAS2367.1.

Yang, D., W. Zhou, and S. D. Seidel, 2022: Substantial influence of vapour buoyancy on tropospheric air temperature and subtropical cloud. *Nat. Geosci.*, **15**, 781–788, https://doi.org/10.1038/s41561-022-01033-x.

Zhang, P., and N. J. Lutsko, 2022: Seasonal superrotation in Earth's troposphere. *J. Atmos. Sci.*, **79**, 3297–3314, https://doi.org/10.1175/JAS-D-22-0066.1.